14 Apr 2013

Electron Loss and Capture from Low-charge-state Oxygen Projectiles in Methane

A. C.F. Santos

W. Wolff

M. M. Sant'Anna

G. M. Sigaud

et. al. For a complete list of authors, see https://scholarsmine.mst.edu/phys_facwork/3098

Recommended Citation

A. C. Santos et al., "Electron Loss and Capture from Low-charge-state Oxygen Projectiles in Methane," *Journal of Physics B: Atomic, Molecular and Optical Physics*, vol. 46, no. 7, article no. 075202, IOP Publishing, Apr 2013.
The definitive version is available at https://doi.org/10.1088/0953-4075/46/7/075202

PAPER

Electron loss and capture from low-charge-state oxygen projectiles in methane

J. Phys. B: At. Mol. Opt. Phys. **46** (2013) 075202 (6pp) doi:10.1088/0953-4075/46/7/075202

Electron loss and capture from low-charge-state oxygen projectiles in methane

A C F Santos[1,4], W Wolff[1], M M Sant'Anna[1], G M Sigaud[2] and R D DuBois[3]

[1] Instituto de Física, Universidade Federal do Rio de Janeiro, PO 68528, 21941-972 Rio de Janeiro, RJ, Brazil
[2] Departamento de Física, Pontifícia Universidade Católica do Rio de Janeiro, Caixa Postal 38071, Rio de Janeiro 22452-970, RJ, Brazil
[3] Department of Physics, Missouri University of Science and Technology, Rolla, MO, USA

E-mail: toni@if.ufrj.br

Received 10 December 2012, in final form 19 February 2013
Published 12 March 2013
Online at stacks.iop.org/JPhysB/46/075202

Abstract
Absolute cross sections for single- and double-electron loss and single- and multiple-electron capture of 15–1000 keV oxygen projectiles ($q = -1, 0, 1, 2$) colliding with the methane molecule are presented. The experimental data are used to examine cross-section scaling characteristics for the electron loss of various projectiles. In addition, a modified version of the free-collision model was employed for the calculation of the single- and total-electron-loss cross sections of oxygen projectiles presented in this work. The comparison of the calculated cross sections with the present experimental data shows very good agreement for projectile velocities above 1.0 au. The comparison of the present single-electron-capture cross sections with other projectiles having the same charge shows good agreement, and a common curve can be drawn through the different data sets.

(Some figures may appear in colour only in the online journal)

1. Introduction

Experimental knowledge about electron loss (projectile ionization/stripping) and capture for collisions of oxygen projectiles with various hydrocarbon molecules are needed for comet and planetary emission modelling codes. For example, oxygen ions in the intermediate velocity regime, produced when the solar plasma impinges onto Titan's rich-in-hydrocarbons-atmosphere (1.5–5.0%), have been observed in Saturn's outer magnetosphere [1–3]. This results in significant ionization, fragmentation and heating of the atmospheric molecules, thus drastically modifying the inventory of the ionospheric chemistry. On the nightside, magnetospheric energetic ions, such as O^+, constitute an important energy source for Titan's upper atmosphere [4]. This study concentrates on interactions with methane as it is one of the major constituents of the upper atmospheres of the outer planets [3].

Projectile electron loss and capture involving oxygen ions are also important reactions for interpreting plasma fusion properties and for the development of laser devices. For instance, in plasma research, spurious carbon and oxygen ions from various parts of the system can cool down the plasma by way of inelastic collisions with atoms and molecules in the plasma [5, 6]. Electron-loss and -capture data also provide benchmarks for theoretical and semi-empirical calculations [5].

For these reasons, projectile-electron-loss and electron-capture experiments have been reported in the literature for collisions of several projectiles with the methane molecule. Sanders *et al* [7] obtained cross sections for electron capture and electron loss from H atoms in collisions with several hydrocarbons. They found that the capture and loss cross sections are contingent on both the number of carbon and

[4] Author to whom any correspondence should be addressed.

hydrogen atoms in the target molecules, as predicted by the additivity (Bragg's) rule. Djurić *et al* [5] measured absolute multiple-electron-capture cross sections between highly charged ions with methane. Sataka *et al* [8] determined single- and double-electron-loss cross sections of He, and single-electron-capture and single-electron-loss cross sections of He^+ in collisions with several molecules, including the methane molecule. They also determined atomic cross sections using Bragg's additivity rule and examined scaling rules for electron-capture cross sections. Rudd *et al* [9] measured cross sections for the production of positive and negative charges as well as projectile electron loss and capture for He^+ on several atomic and molecular (including methane) targets. Varghese *et al* [10] measured single-electron-capture cross sections for H^+ from several gases. Their systematic measurements display additivity failure in some molecular species. They also used a simple geometrical model to estimate intramolecular electron-loss probabilities, which allowed the extraction of atomic values at each projectile energy. Rottman *et al* [11] determined single-electron-capture cross sections for C^+ impact on several targets. For the atomic targets, the single-electron-capture cross sections were found to merge as the impact energy increased. Their single-electron-capture cross sections were found to scale with the square of the bond length for the diatomic targets and with the number of atoms comprising the polyatomic targets.

But even after decades of research and the large database of electron-loss and electron-capture information available, data for many systems of interest are still limited. On the other hand, theoretical studies which try to take into account the several processes involved in the dynamics of collisions of multi-electronic projectiles and atoms and molecules in the low- to intermediate-velocity regime are even scarcer. For these reasons, several efforts concerning scaling laws for single- and multiple-electron loss have been reported [12–16]. The formulas are considered to have predictive capabilities with accuracy within a factor of 2. The target dependence for projectile electron loss has also been investigated [17]. For energies less than several MeV/u, the target dependences were shown to be very similar, independent of projectile species and charge state [17].

Sigaud employed the free-collision classical-impulse model in the calculation of the screening contribution to the total electron-loss cross sections of several anions (B^-, C^-, O^-, F^-, Al^-, S^- and Cl^-) in collision with noble gases [18]. This model was then extended for projectiles with two or more electrons in the same subshell, such as He^0, B^+ and C^{2+}, and applied to the determination of the screening part of the total electron-loss cross sections of not only these projectiles but also H^-, He^-, B^{2+}, C^+, C^{3+} and O^{5+} colliding with H_2 molecular targets [19]. In all calculations, the multi-electronic quality of the projectile was taken into account within the independent particle model (IPM).

In this paper, we report absolute cross sections for single- and double-electron loss and single- and multiple-electron capture of 15−1000 keV oxygen projectiles ($q = -1, 0, 1, 2$) colliding with the CH_4 molecule. In addition, calculations were performed using both an extended

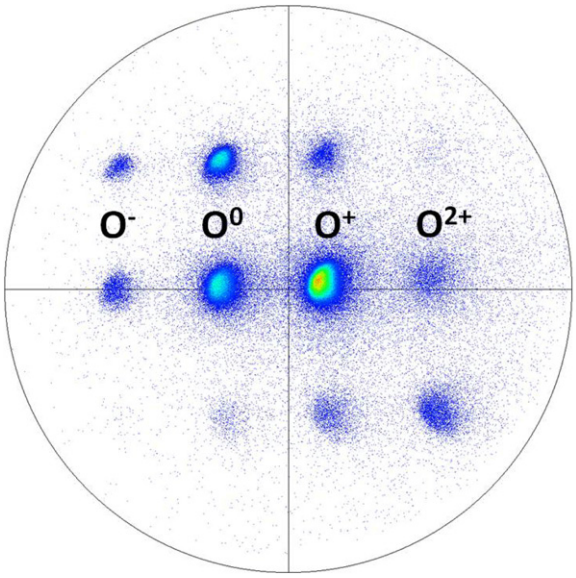

Figure 1. Two-dimensional image from the position-sensitive detector at the end of the beamline. The most intense island near the centre of the detector is the 200 keV O^+ main beam.

version of the classical-impulse free-collision model and the plane-wave Born approximation (PWBA). Methane is a highly symmetrical molecule (T_d point group), in the ground electronic state ($X\ A_1$).

2. Experiment

Oxygen beams ($q = -1, 0, +1, +2$) with energies ranging from 15−1000 keV were produced from O^- beams, provided by the 1.7 MV tandem accelerator at the Federal University of Rio de Janeiro (UFRJ) [20–25]. The negative beams cross the stripper N_2 cell, where they can lose electrons, the number depending on the gas pressure. The emergent beams are selected in momentum by an analysing magnet and guided into the beamline, held at 10^{-8} Torr. A parallel-plate electrostatic analyser, settled downstream from a collimator set, is placed before the entrance of the target cell. The analyser provides a transverse electric field which separates the desired incident charge states from spurious beams generated by collisions of the main beam with the residual gas. The beam is then delivered to a 12 cm long differentially pumped target gas cell. The pressure in the target cell is measured with an accuracy of 5% by an absolute capacitive manometer. The separation of the different charge states of the beam emerging from the target cell is performed by a second electrostatic analyser, located after the cell. The different charge states are detected by an *xy*-position-sensitive detector located at the end of the beamline. The projectile detector comprises a microchannel plate in a chevron configuration and a resistive anode. The position-sensitive detector permits easy recognition of spurious beams as shown in figure 1. For the energies used, it was assumed that the detection efficiency was independent of either the charge state or the energy of the particle hitting the detector [26], so that the ratio of counting rates is a measure of the ion intensity ratio. The absolute cross sections, σ_{ij}, where i and j represent the initial and final projectile charge states,

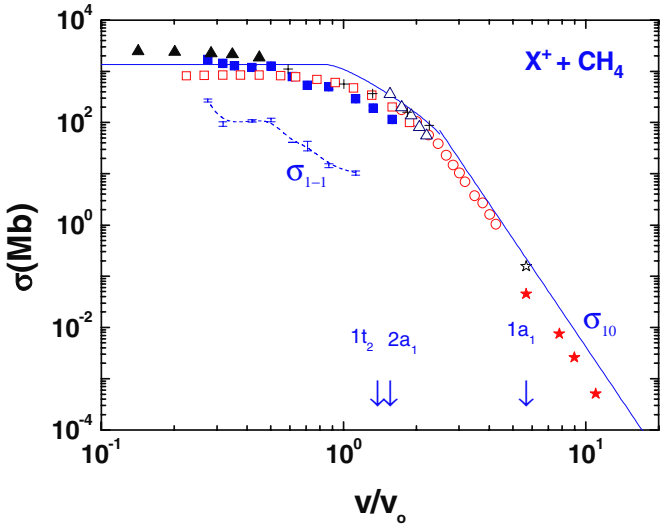

Figure 2. Single- and double-electron capture of singly charged projectiles from CH_4 as a function of the projectile velocity in atomic units ($v_o = c/137$, where c is the speed of light in vacuum). Single capture: closed squares, O^+ (this work); closed triangles, H^+ [29]; open circles, He^+ [8]; closed stars, H^+ [7]; open star, He^+ [9]; open squares, He^+ [9]; open triangles, H^+ [7]; crosses, C^+ [11]; dashed line: double capture of O^+ (this work); full line, semi-classical Bohr–Lindhard model (with $Z_2 = 10$, $\alpha = 1$, $I_a = 14.25$ eV ($1t_1$) [27]) [28]. The vertical arrows indicate the average electron speed in a given molecular orbital [27].

respectively, were determined using the growth-rate method [20].

3. Results

Using the methods outlined above, absolute cross sections were measured for total, single- and multiple-projectile-electron loss and single- and double-electron capture for O^-, O°, O^+ and O^{2+} ions colliding with methane which are tabulated in tables 1–3 and shown graphically in figures 2–5. The tabulated cross sections are in units of Mb (10^{-18} cm^2) with the combined uncertainties obtained in a linear fitting to the data and from extracting the peak counts.

3.1. O^+ cross sections

The O^+ projectile has three ($2s^22p^3$) electrons in its outermost shell ($I_p = 35.1$ eV) [27]; the ground state is ($^4S_{3/2}$). Like other open shell atoms and ions, O^+ has two low-lying (close to the ground state term) metastable excited states with the same electronic configuration, $(2s^22p^3)\,^2D_{5/2,3/2}$ and $(2s^22p^3)\,^2P_{3/2,1/2}$, with lifetimes of approximately 3.6 h and 5 s, respectively [28, 29]. In the present study, the condition $\tau v > l$ is always fulfilled, where τ is the lifetime of the excited state, v is the projectile velocity and l is the distance travelled by the projectile from the place it is formed to the collision region. So, we cannot separate those metastable states in the present measurements. The present results indicate, however, that the differences between the electron-capture cross section for the projectile in the ground and the excited states are fairly small, or also indicate that very few metastables are formed, because the single-electron-capture cross sections do not differ from the general trend for singly charged projectiles as shown in figure 2. On the other hand, the production of metastable projectiles is energy dependent and decreases as the projectile velocity increases. The single- and double-electron-capture cross sections for O^+ from methane from the present measurements, σ_{10} and σ_{1-1}, respectively, are plotted as a function of the projectile velocity in figure 2, together with data for singly charged projectiles, H^+ [7, 10, 30], He^+ [8, 9], C^+ [11] and a theoretical estimate using the semi-classical Bohr–Lindhard model by Knudsen *et al* [31] with the adjustable parameter $\alpha = 1$, which is based on a classical description of electron capture from atomic targets. We have adopted the target effective atomic number defined as $Z_{\rm eff} = \Sigma_i Z_i$ [32]. The comparison of the present single-electron-capture data with those previously published data for other singly charged projectiles shows good agreement, and a common curve can be drawn through the data sets. The agreement between Knudsen's estimate and experiment is quite good. At higher energies the Bohr–Lindhard model overestimates the cross sections, which can be attributed to two reasons: in the intermediate velocity regime, the probability of projectile electron loss is of the same order or higher than the electron-capture probability. As a consequence, the probabilities for the several channels are no longer independent. In this situation, the coupling of these channels has to be taken into account for a correct description of the problem [33]. Another reason is the failure of the description of the target electron velocity distributions in Knudsen's model. The vertical arrows in figure 2 indicate the average electron orbital speed in a given molecular orbital [27]. On the other hand, the experimental data have the same dependence with the projectile velocity (v^{-7}) as predicted by the simple estimate given by the Bohr–Lindhard model. We are not aware of any data for double-electron capture from methane in the literature.

The total-projectile-electron-loss ($\sigma_{\rm tot}$), single-projectile-electron-loss (σ_{12}) and double-projectile-electron-loss (σ_{13}) cross sections for O^+ from methane from the present measurements are plotted as a function of the projectile energy

Table 1. Absolute single- and double-projectile-electron-loss cross sections and single- and double-electron-capture cross sections in Mb for O^+ projectiles in methane as a function of the projectile energy, E, in keV.

Energy (keV)	σ_{12} (Mb)	σ_{13} (Mb)	σ_{10} (Mb)	σ_{1-1} (Mb)
30	–	–	1698 ± 100	270 ± 27
40	–	–	1425 ± 100	94 ± 10
50	–	–	1280 ± 120	–
70	–	–	1182 ± 100	108 ± 11
100	–	–	1266 ± 100	113 ± 10
150	17.6 ± 3.1	–	789 ± 30	41.2 ± 4.0
200	33.2 ± 3.3	–	535 ± 54	35.4 ± 7.2
300	119 ± 12	–	495 ± 50	14.4 ± 1.3
500	213 ± 20	–	288 ± 29	10.4 ± 1.0
700	265 ± 27	37 ± 4	191 ± 20	–
1000	306 ± 30	58.3 ± 4.0	114 ± 11	–

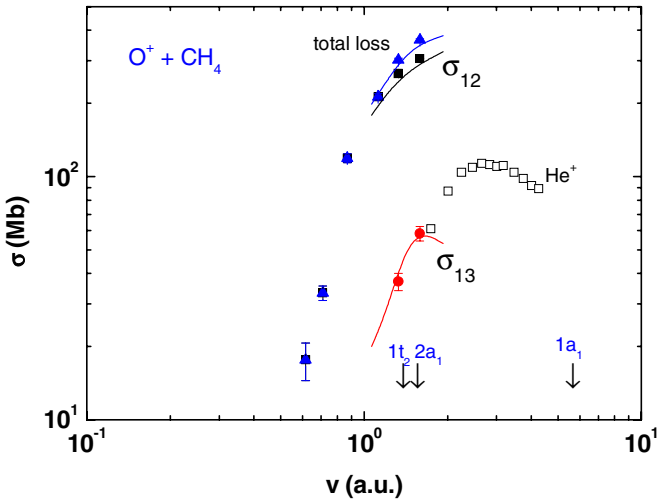

Figure 3. Electron loss cross section for $O^+ + CH_4$ as a function of the projectile velocity in atomic units. Experiment: open and filled squares, single-electron loss; filled circles, double-electron loss; filled triangles, total (single + double) electron loss; open squares, single-electron loss for He^+ [9]. Theory: solid lines, free-collision model. The vertical arrows indicate the average electron speed in a given molecular orbital [27].

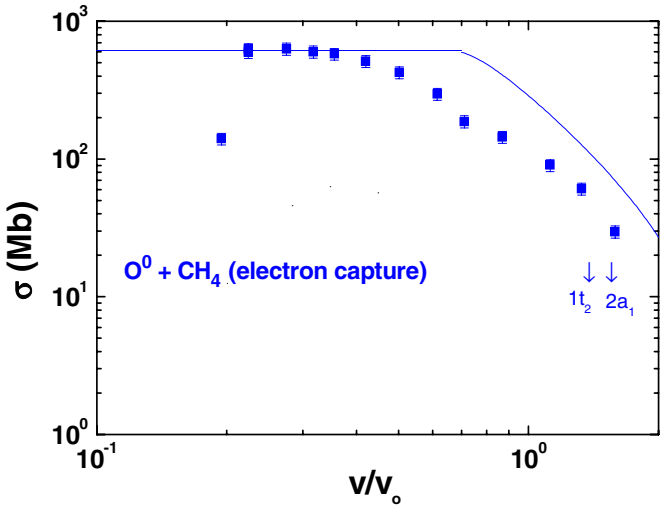

Figure 4. Single-electron capture of O^0 projectiles from CH_4. Single capture: closed squares, this work; full line, semi-classical Bohr–Lindhard model [28].

in figure 3, together with the present theoretical calculations. In the velocity range of the present measurements the electron loss is dominated by the screening mode (interaction between the projectile active electrons and the screened target nucleus), since the anti-screening mode (interaction between the projectile active electrons and those of the target) begins to contribute to the electron loss cross sections for energies above 0.8 MeV for O^0 and 1.4 MeV for O^+ projectiles [34, 35]. The screening contribution to the electron loss was computed using the extended classical-impulse free-collision model as proposed by Sigaud [18, 19]. In this model, the active projectile electron is dealt with as a free electron, which is elastically scattered by the target atom. The screening contribution to the electron loss cross section is found by integrating the electron elastic differential cross sections over the scattering angle. It should be noted that the calculations based on the free-collision model are restricted to projectile velocities larger than the orbital velocities of the projectile active electrons [18, 19]. Due to this constraint, we have limited the present calculations to the O^0 and O^+ projectiles, and, even for them, we could not cover the whole range of velocities of the present measurements.

In the present calculations, the elastic differential cross sections from Curry *et al* (measured) [36] and from Bettega *et al* [37] and Machado *et al* [38] (calculated) were used for low-energy electrons, and those from Iga *et al* (measured and calculated) [39] for high-energy electrons. The calculated electron-loss cross sections presented variations smaller than 10% in the energy regions where these sets of data overlap for both projectile charge states. Some remarks can be made from figure 3. First, the results obtained in the free-collision model are in close agreement with the experimental data for single-, double- and total-electron-loss cross sections. Second, both the measured and calculated cross sections for single- and double-electron-loss increase as a function of the projectile velocity up to 1.5 au, around the average velocities of the $1t_2$ and $2a_1$ target electrons where the cross sections are supposed to maximize.

3.2. O^0 cross sections

The O^0 projectile has four electrons in its outermost shell ($1s^2 2s^2 2p^4, {}^3P$) ($I_p = 13.590$ eV) [40]. The average kinetic energy of the 2p electrons in oxygen is $U = 69.636$ eV [41]. However, some metastables, $O(^1D)$ and $O(^1S)$, may also contribute to the O^0 beam. The use of N_2 as a stripper is expected to produce mainly a $O(^3P)$ O^0 beam [42]. The single-electron-capture cross sections for O^0 from methane from the present measurements, $\sigma_{0\text{–}1}$, are plotted as a function of the projectile velocity in figure 4, together with the theoretical estimate using the semi-classical Bohr–Lindhard model with the adjustable parameter $\alpha = 1$. The captured electron is likely to be one of the six outermost electrons in the methane molecule from the $1t_2$ orbital (binding energy = 14.25 eV, average kinetic energy = 25.96 eV) [41]. Like the O^+ case, the agreement between Knudsen's estimate for the single-electron-capture cross sections and experiment is very good at low projectile velocities ($v \leqslant 0.35\ v_0$) where the cross sections are roughly independent of the projectile velocity, but deviates at intermediate velocities ($0.35 \leqslant v \leqslant 1.0$) for a projectile effective charge $q_{\text{eff}} = 0.4$. The only other electron-capture data with which the present results may be directly compared are those of Lindsay *et al* for H^0 [30]. The H^0 data (not shown in figure 4) are one order of magnitude lower than the present results. The reason for this difference is not understood. One of the critical distances in the Bohr–Lindhard model is the release radius, the distance in which the Coulomb force from the projectile is equal to the binding force of the electron in the target. From the present data, the release radius can be estimated as $R_R = (\sigma_{0\text{–}1}/\pi)^{1/2} \cong 23$ au. Again, we are not aware of any other data for electron capture of neutral projectiles on methane.

Table 2. Absolute single-projectile-electron-loss (σ_{01}), double-projectile-electron-loss (σ_{02}), triple-projectile-electron-loss (σ_{03}) cross sections and single-electron capture (σ_{0-1}) cross sections in Mb for O^0 projectiles in methane as a function of the projectile energy, E.

Energy (keV)	σ_{01} (Mb)	σ_{02} (Mb)	σ_{03} (Mb)	σ_{0-1} (Mb)
15	–	–	–	140.0 ± 5.6
20	–	-	–	613 ± 84
30	–	-	–	632 ± 60
40	61.5 ± 6.0	-	–	601 ± 60
50	83.0 ± 9.0	–	–	579 ± 60
70	131 ± 13	–	–	513 ± 51
100	220 ± 20	–	–	425 ± 40
150	333 ± 30	–	–	296 ± 30
200	464 ± 46	87 ± 20	–	187 ± 19
300	535 ± 50	108 ± 10	–	144 ± 14
500	580 ± 58	143 ± 14	14.7 ± 3.2	90.1 ± 9.0
700	598 ± 60	164 ± 18	30.6 ± 2.0	60.8 ± 6.0
1000	567 ± 30	202 ± 25	42.9 ± 4.0	29.6 ± 3.0

The total-projectile-electron-loss (σ_{tot}), single-projectile-electron-loss (σ_{01}) and double-projectile-electron-loss (σ_{02}) cross sections for O^0 from methane from the present measurements are plotted as a function of the projectile energy in figure 5, together with the experimental data for H^0 projectiles [7], He^0 [8] and the free-collision model calculations. Because of the number of available projectile electrons and their lower binding energies, the electron-loss cross section for neutral projectiles is larger than the corresponding cross sections for singly charged projectiles shown in figure 3. From figure 5, we observe that the projectile-loss cross sections increase with the projectile velocity up to a maximum at a characteristic velocity. In a first-order approximation, this characteristic velocity is expected to match the velocity of the most loosely bound electron of the projectile. Above that characteristic velocity, the cross section decreases slowly as a function of the projectile velocity. In fact, figure 5 shows that the loss cross section of O^0 has a maximum around $v = 1.6$ au, the mean velocity of the 2p electron in the O^0 [43], indicated in figure 5 by a vertical dotted line.

The data for H^0 are slightly smaller than the present data for O^0, as expected from the scaling law of Santos and DuBois [12] which predicts that the electron loss cross sections scale as $\sigma \sim N_{\rm eff}^{0.4}/I_p$, where $N_{\rm eff}$ is the effective number of the outermost electrons in the projectile and I_p is the projectile ionization potential. Again, the results obtained in the free-collision model are in close agreement with the experimental data for single-, double- and total-electron-loss cross sections. The single-electron-loss cross sections for neutral oxygen beams in methane maximizes near 1.0 MeV where it is responsible for 72% of the total projectile electron loss cross section. The measured absolute cross sections for electron capture and loss of O^0 in methane are shown in table 2.

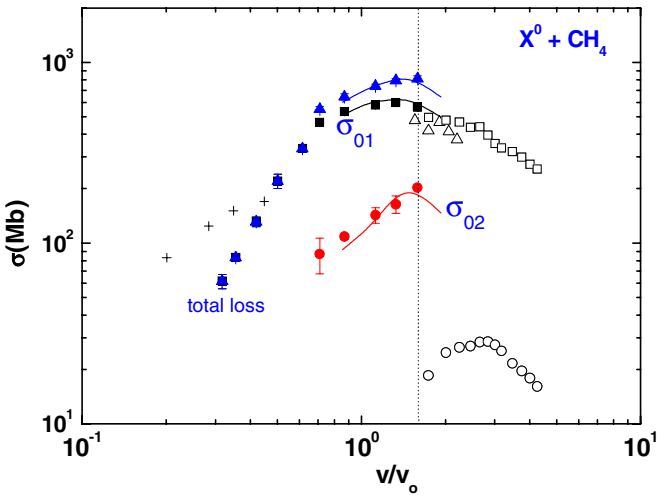

Figure 5. Electron-loss cross section for $O^0 + CH_4$ as a function of the projectile energy. Experiment: filled triangles, squares and circles, total, single- and double-electron loss from O^0 (this work); full lines (theory for total, single- and double-electron loss from O^0 this work); open triangles and squares, single-electron loss from H^0 (ref. [7]) and He^0 [8]; crosses, electron loss from H^0 [30]; open circles, double-electron loss from He^0 [8]. The vertical dotted line indicates the velocity of the most loosely bound electron in the O° projectile [42]. The low-energy data for the total- and single-electron loss are the same.

3.3. O^- and O^{2+} cross sections

Table 3 presents the measured projectile-electron-loss and -capture cross section of the O^- and O^{2+} beam from methane. Due to the experimental limitations, the cross sections were obtained for a short range of projectile velocities and are provided only in a tabular form.

The cross section for a projectile of charge q to capture an electron from the target at a given projectile velocity is expected to increase with q. In fact, the capture cross section of O^{2+} from methane is roughly twice the corresponding capture cross section of O^+ at the same projectile velocity, as predicted by the semi-classical Bohr–Lindhard model. On the other hand, the multiple-electron-capture cross sections decrease roughly one order of magnitude for each extra electron captured.

The electron loss cross sections for O^- are larger than the accompanying cross sections of O^+ and O^0 as expected.

Table 3. Absolute single-, double- and triple-electron-capture cross sections in Mb for O^{2+} projectiles, and single-electron loss for O^- projectiles in methane as a function of the projectile energy, E.

$O^{2+} + CH_4$				$O^- + CH_4$	
Energy (keV)	Single capture (Mb)	Double capture (Mb)	Triple capture (Mb)	Energy (keV)	Single loss σ (Mb)
200	(106 ± 10) × 10	184 ± 33	16.0 ± 2.4	15	258 ± 26
300	(98 ± 10) × 10	148 ± 15	14.7 ± 2.3	20	426 ± 50

4. Conclusions

We have measured absolute cross sections for the total projectile single- and double-electron loss and single- and double-electron capture of oxygen projectiles colliding with the methane molecule, in the energy range from 15 to 1000 keV, with the objective of providing benchmark data of interest not only to applications in, among other fields, plasma physics and astrophysics, but also to increase the available absolute data for comparison with theoretical models which try to describe the complex dynamics of collisions between many-electron projectiles and atoms and molecules.

The present data for single-electron capture of O^+ projectiles have been compared with the data available in the literature for singly charged projectiles colliding with the same target. There is good agreement between the present set of data and the previous data for the single-electron capture by singly charged projectiles, but the experimental data lie, in general, well below the theoretical estimate using the Bohr–Lindhard model.

In the case of projectile electron loss, the present data were compared with the free-collision classical-impulse model for the calculation of the screening contribution to the single- and total-electron-loss cross sections. The multi-electronic character of the projectiles was taken into account within the independent particle model (IPM). Very good agreement was found between the present set of data and the previous data for the single- and total-electron loss by singly charged fragments,

Acknowledgments

This work was supported in part by the Brazilian agencies CNPq and FAPERJ.

References

[1] Sittler E C, Ali A, Cooper J F, Hartle R E, Johnson R E, Coates A J and Young D T 2009 *Planet. Space Sci.* **57** 1547
[2] Luhmann J G *et al* 2006 *Icarus* **181** 465
[3] Mount G H, Warden E S and Moos H W 1977 *Astrophys. J.* **214** L47
[4] Lavvas P, Galand M, Yelle R V, Heays A N, Lewis B R, Lewis G R and Coates A J 2011 *Icarus* **213** 233
[5] Djurić N, Smith S J, Simcic J and Chutjian A 2008 *Astrophys. J.* **679** 1661–4
[6] Tawara H and Fritsch W 1989 *Phys. Scr.* **T28** 58
[7] Sanders J M, Varghese S L, Fleming C H and Soosai G A 2003 *J. Phys. B: At. Mol. Opt. Phys.* **36** 3835
[8] Sataka M, Yagishitat A and Nakai Y 1990 *J. Phys. B: At. Mol. Opt. Phys.* **23** 1225
[9] Rudd M E, Goffe T V, Itoh A and DuBois R D 1985 *Phys. Rev.* A **32** 829
[10] Varghese S L, Bissinger G, Joyce J M and Laubert R 1985 *Phys. Rev.* A **31** 2202
[11] Rottmann L, Bruch R, Neil P, Drexler C, DuBois R D and Toburen L H 1992 *Phys. Rev.* A **46** 3883
[12] Santos A C F and DuBois R D 2004 *Phys. Rev.* A **69** 042709
[13] DuBois R D, Santos A C F and Olson R E 2005 *Nucl. Instrum. Methods* A **544** 497
[14] Shevelko V P *et al* 2010 *J. Phys. B: At. Mol. Opt. Phys.* **43** 215202
[15] Song M Y, Litsarev M S and Shevelko V P 2009 *Nucl. Instrum. Methods* B **267** 2369
[16] Shevelko V P *et al* 2009 *J. Phys. B: At. Mol. Opt. Phys.* **42** 065202
[17] DuBois R D, Santos A C F, Sigaud G M and Montenegro E C 2011 *Phys. Rev.* A **84** 022702
[18] Sigaud G M 2008 *J. Phys. B: At. Mol. Opt. Phys.* **41** 015205
[19] Sigaud G M 2011 *J. Phys. B: At. Mol. Opt. Phys.* **44** 225201
[20] Wolff W, Luna H, Santos A C F, Montenegro E C and Sigaud G M 2009 *Phys. Rev.* A **80** 032703
[21] Sant'Anna M M *et al* 2009 *Phys. Rev.* A **80** 042707
[22] Wolff W, Luna H, Santos A C F, Montenegro E C, DuBois R D, Montanari C C and Miraglia J E 2011 *Phys. Rev.* A **84** 042704
[23] Sant'Anna M M, Zappa F, Jalbert G, Santos A C F, Magnani B F, Coelho L F S and Faria N V C 2009 *Plasma Phys. Control. Fusion* **51** 045007
[24] Sant'Anna M M, Zappa F, Santos A C F, de Barros A L F, Wolf W, Coelho L F S and de Castro Faria N V 2006 *J. Physique IV* **133** 757
[25] Sant'Anna M M, Zappa F, Santos A C F, Coelho L F S, Wolff W, Barros A L F and de Castro-Faria N V 2006 *Phys. Rev.* A **74** 022701
[26] Santos A C F, Melo W S, Sant'Anna M M, Sigaud G M and Montenegro E C 2002 *Rev. Sci. Instrum.* **73** 2369
[27] Electron-impact ionization cross sections http://physics.nist.gov/
[28] Kim Y-K and Desclaux J-P 2002 *Phys. Rev.* A **66** 012708
[29] Lindsay B G, Merrill R L, Straub H C, Smith K A and Stebbings R F 1998 *Phys. Rev.* A **57** 331
[30] Lindsay B G, Yu W S and Strebbings R F 2005 *J. Phys. B: At. Mol. Opt. Phys.* **38** 1977
[31] Knudsen H, Haugen H K and Hvelplund P 1981 *Phys. Rev.* A **23** 597
[32] Watson R L, Peng Yong, Horvat V and Kim G J 2003 *Phys. Rev.* A **67** 022706
[33] Melo W S, Sant'Anna M M, Santos A C F, Sigaud G M and Montenegro E C 1999 *Phys. Rev.* A **60** 1124
[34] McGuire J H, Stolterfoht N and Simony P R 1981 *Phys. Rev.* A **24** 97
[35] Montenegro E C, Meyerhof W E and McGuire J H 1994 *Adv. At. Mol. Opt. Phys.* **34** 250
[36] Curry P J, Newell W R and Smith A C H 1985 *J. Phys. B: At. Mol. Phys.* **18** 2303
[37] Bettega M H F, Natalense A P P, Lima M A P and Ferreira L G 1995 *J. Chem. Phys.* **103** 10566
[38] Machado L E, Lee M-T and Brescansin L M 1998 *Braz. J. Phys.* **28** 111
[39] Iga I, Lee M-T, Homem M G P, Brescansin L M and Machado L E 2000 *Phys. Rev.* A **61** 022708
[40] Carlson T A, Nestor C W Jr, Wasserman N and McDowell J D 1970 *At. Data* **2** 63
[41] Kim Y-K, Hwang W, Weinberger N M, Ali M A and Rudd M E 1997 *J. Chem. Phys.* **106** 1026
[42] Lindsay B G, Yu W S, McDonald K F and Strebings R F 2004 *Phys. Rev.* A **70** 042701
[43] Kim Y-K and Desclaux J-P 2002 *Phys. Rev.* A **66** 012708